Dissipative structure and long term behavior of a finite element approximation of incompressible flows with numerical subgrid scale modeling

Ramon Codina, Javier Principe and Santiago Badia

Universitat Politècnica de Catalunya
ramon.codina@upc.edu, principe@cimne.upc.edu, sbadia@cimne.upc.edu

1 Introduction

The objective of this paper is to summarize the finite element formulation for incompressible flows that has been developed in our group during the last years, starting with [7], and also to present some of the latest results [12, 10, 23, 15, 2]. In particular, issues related to stability, the dissipative structure of the formulation, the energy transfer between unresolved and resolved scales (including a discussion about the possibility to produce backscatter) and the long term behavior will be addressed. Our purpose is to explain the main ideas without technicalities, even at the expense of some occasional lack of precision. Likewise, we do not pretend to be exhaustive in the bibliographical references. The reader is addressed to the bibliography included in the papers listed above for more details.

The formulation we will present can be framed within the variational multiscale concept introduced in [17, 18]. In fact, the starting point is a *two scale* decomposition of the unknowns, the velocity $\boldsymbol{u}$ and the pressure p, defined in a spatial domain Ω and in a time interval $[0, T]$, including the possibility to let $T \to \infty$. The original motivation of this type of formulations was to justify the so called *stabilized finite element methods*. In the case of the incompressible Navier-Stokes equations, stabilization is required to avoid the need for using velocity-pressure interpolations satisfying the inf-sup condition and to deal with convection-dominated flows (see, for example, [5, 14] for an overview of different methods and background).

Let V and Q be the spaces where velocities and pressures must belong for $t \in [0, T]$. In all what follows, the time variable will be left continuous. Regularity in time of the unknowns will be specified when required. Let also $V_h \subset V$ and $Q_h \subset Q$ be finite element spaces to approximate the velocity and the pressure, respectively, *in space*.

The starting idea of the formulation to be presented is to split the velocity and the pressure as

$$\boldsymbol{u} = \boldsymbol{u}_h + \tilde{\boldsymbol{u}}, \quad p = p_h + \tilde{p}, \tag{1}$$

where $\boldsymbol{u}_h$, p_h belong to the finite element spaces and $\tilde{\boldsymbol{u}}$ and $\tilde{p}$ are what we will call the subgrid scales or, simply, *the subscales*. The way these are modeled defines the particular numerical approximation. We can identify the finite element components of the solution as the *resolved* scales, whereas the subscales are the *unresolved* scales.

Splitting (1) is usually used together with several approximations when stabilized finite element methods need to be justified. However, our approach is to accept the multiscale decomposition with *all its consequences* and, in particular:

- To consider the subscales to be time dependent.
- To keep the nonlinear terms involving $\tilde{\boldsymbol{u}}$ in the Navier-Stokes equations.

Both items will be described in what follows. Some of the rewards are

- The dependence of the subscales with the time step size of the time integration scheme becomes clear.
- Global conservation of momentum can be obtained.
- Modeling of the subcales defines automatically a model for the extra stresses appearing in a LES-like approach .

The first two issues are discussed in detail in [12] (see also references therein). The third item will be also discussed here.

Let us analyze the implications of keeping the nonlinear terms involving $\tilde{\boldsymbol{u}}$ in the Navier-Stokes equations. Using (1), the convective term will lead to

$$\begin{aligned} \nabla\cdot(\boldsymbol{u}\otimes\boldsymbol{u}) &= \nabla\cdot(\boldsymbol{u}_h\otimes\boldsymbol{u}_h) + \nabla\cdot(\boldsymbol{u}_h\otimes\tilde{\boldsymbol{u}}) + \nabla\cdot(\tilde{\boldsymbol{u}}\otimes\boldsymbol{u}_h) + \nabla\cdot(\tilde{\boldsymbol{u}}\otimes\tilde{\boldsymbol{u}}) \\ &\equiv \text{(I)} + \text{(II)} + \text{(III)} + \text{(IV)}. \end{aligned} \tag{2}$$

Obviously, (I) would be the only term appearing in a Galerkin approximation, whereas the rest are the contributions from the velocity subscale. It can be shown that when this subscale is modeled, the term that provides numerical stability is (II), in the sense that it allows control of the convective derivative and the pressure gradient, in order to deal with convection dominated flows. One can also show that (III) leads to global momentum conservation [12].

Because of its resemblance with similar terms in turbulence models, (IV) in (2) raises the question of whether keeping the contribution from the subscales in the convective term could be viewed as a turbulence model or not. This possibility was mentioned in [7], which contrasts with the option in [19], where a large-eddy-simulation (LES) model is used to represent the subgrid scales (see Remark 6 in [7] and, for background on LES models, [22]). In [3] the possibility to model turbulence using only numerical ingredients within the

variational multiscale context is fully and successfully exploited. The role of numerical stabilization terms as turbulence models was also envisaged in [13, 16], for example.

By analogy with LES models, the different terms appearing in (2) could be termed as follows:

$$\begin{aligned} \text{(II)+(III)} \quad &= \boldsymbol{u}_h \otimes \tilde{\boldsymbol{u}} + \tilde{\boldsymbol{u}} \otimes \boldsymbol{u}_h : \quad \text{Cross stress} \\ \text{(IV)} \quad &= \tilde{\boldsymbol{u}} \otimes \tilde{\boldsymbol{u}} \quad : \quad \text{Reynolds stress} \\ \text{(II)+(III)+(IV)} \quad &= \boldsymbol{u}_h \otimes \boldsymbol{u}_h - \boldsymbol{u} \otimes \boldsymbol{u} : \quad \text{Subgrid scale tensor} \end{aligned}$$

Some comments in the line of viewing an approximation to the subscales in (2) as an effective LES model will be provided in the following.

The other crucial point of our approach is to keep the time dependency of the velocity subscale. Thus, the velocity time derivative can be split as

$$\partial_t \boldsymbol{u} = \partial_t \boldsymbol{u}_h + \partial_t \tilde{\boldsymbol{u}}. \tag{3}$$

The first term would be the only one kept if the time derivative of the subscales is neglected. In this situation, the subscales were termed *quasi-static* in [7], in contrast to *dynamic subscales* if they are considered to be time-dependent. As shown in [12], the second term leads to a correct behavior of time integration schemes and better accuracy. In particular, in [1] stability and convergence for the Stokes problem is proved without any restriction on the time step size and the stabilization parameters on which the formulation depends.

The third crucial ingredient does not follow from assuming the consequences of the two-scale decomposition, but from the choice of the space for the subscales. As explained later, our analysis relies heavily on the fact that we consider this space orthogonal to the finite element space.

As indicated earlier, apart from presenting the numerical formulation we propose, which is described in Section 2, our purpose is to discuss issues related to its dissipative structure and its long term behavior. Let us summarize the main results to be explained.

Assuming that

- orthogonal subgrid scales are used,
- the finite element mesh is capable of capturing (part of) the inertial range,
- the assumptions of classical statistical fluid mechanics apply,

one can show that *the dissipation introduced by (II) + (III) in (2) is proportional to the molecular dissipation of the physical subgrid scales*. The meaning of the assumptions listed and the above conclusion is explained in Section 3.

Also in Section 3 we will state the energy budget presented in [23]. We will show that *the finite element component and the subgrid component have a proper scale separation only if they are orthogonal*, in the sense that the total kinetic energy is the sum of the kinetic energy of $\boldsymbol{u}_h$ plus the kinetic energy of $\tilde{\boldsymbol{u}}$. We will also explain why *dynamic subscales ($\partial_t \tilde{\boldsymbol{u}} \neq \boldsymbol{0}$) are needed to model backscatter*.

In Section 4 we will list the results of the long term stability analysis conducted in [2]. We will see that *dynamic subscales allow us to obtain the correct long term stability of the space-discrete scheme.*

Some numerical simulations, which try to show that the numerical model we propose can be used in real applications and has the correct behavior, are presented in Section 5. A summary and some concluding remarks close the paper in Section 6.

2 Formulation

In this section we summarize the formulation we propose. For more details, including bibliographical references, see [7, 12].

2.1 Continuous problem

The Navier-Stokes problem for an incompressible fluid consist of finding a velocity $\boldsymbol{u}$ and a pressure p solution of the initial and boundary value problem

$$\begin{aligned} \partial_t \boldsymbol{u} + \boldsymbol{u}\cdot\nabla\boldsymbol{u} - \nu\Delta\boldsymbol{u} + \nabla p = \boldsymbol{f} \quad & \text{in } \Omega,\ t>0, \\ \nabla\cdot\boldsymbol{u} = 0 \quad & \text{in } \Omega,\ t>0, \\ \boldsymbol{u} = \boldsymbol{0} \quad & \text{on } \Gamma,\ t>0, \\ \boldsymbol{u} = \boldsymbol{u}^0 \quad & \text{in } \Omega,\ t=0. \end{aligned}$$

In these equations, ν is the kinematic viscosity, $\boldsymbol{f}$ is the vector of body forces, $\boldsymbol{u}^0$ is the initial condition and $\Gamma = \partial\Omega$.

Let $V = H^1_0(\Omega)^d$ and $Q = L^2_0(\Omega)$ (L^2 functions with zero mean), d being the number of space dimensions. Let us denote by $(\cdot,\cdot)$ the L^2 inner product in Ω and by $\langle f, g\rangle$ the integral of two functions f and g over Ω, whenever this integral makes sense. When the integral is computed over a region ω, we will denote it as $\langle f, g\rangle_\omega$. Let also $L^2(0,T;V)$ be the set of functions whose V-norm in space is L^2 in time and $\mathcal{D}'(0,T;Q)$ the set of "functions" whose Q-norm in space is a distribution in time. The weak form of the Navier-Stokes equations can be written as follows: find $[\boldsymbol{u}, p] \in L^2(0,T;V)\times\mathcal{D}'(0,T;Q)$ such that

$$(\partial_t\boldsymbol{u},\boldsymbol{v}) + \langle\boldsymbol{u}\cdot\nabla\boldsymbol{u},\boldsymbol{v}\rangle + \nu(\nabla\boldsymbol{u},\nabla\boldsymbol{v}) - (p,\nabla\cdot\boldsymbol{v}) = \langle\boldsymbol{f},\boldsymbol{v}\rangle, \quad \forall\boldsymbol{v}\in V, \tag{4}$$

$$(q,\nabla\cdot\boldsymbol{u}) = 0, \qquad \forall q\in Q. \tag{5}$$

2.2 Subgrid scale decomposition

Let us consider a finite element partition $\{K\}$ of the computational domain Ω. As explained earlier, the starting point of the formulation to be presented is the splitting (1). For simplicity, we will not consider pressure subscales (see [6, 7] for an analysis of their inclusion). Thus, if $\tilde{\boldsymbol{u}}$ is a certain approximation to

the exact velocity subscale, the splitting we consider is $\boldsymbol{u} \approx \boldsymbol{u}_* := \boldsymbol{u}_h + \tilde{\boldsymbol{u}},\ p \approx p_h$. When inserted into (4)-(5) this yields:

$$
\begin{aligned}
&(\partial_t \boldsymbol{u}_h, \boldsymbol{v}_h) + \langle \boldsymbol{u}_* \cdot \nabla \boldsymbol{u}_h, \boldsymbol{v}_h \rangle + \nu(\nabla \boldsymbol{u}_h, \nabla \boldsymbol{v}_h) - (p_h, \nabla \cdot \boldsymbol{v}_h) + (q_h, \nabla \cdot \boldsymbol{u}_h) \\
&\quad + (\partial_t \tilde{\boldsymbol{u}}, \boldsymbol{v}_h) - \sum_K \langle \tilde{\boldsymbol{u}}, \boldsymbol{u}_* \cdot \nabla \boldsymbol{v}_h + \nu \Delta \boldsymbol{v}_h + \nabla q_h \rangle_K \\
&\quad + \sum_K \langle \tilde{\boldsymbol{u}}, \nu \boldsymbol{n} \cdot \nabla \boldsymbol{v}_h + q_h \boldsymbol{n} \rangle_{\partial K} = \langle \boldsymbol{f}, \boldsymbol{v}_h \rangle, \qquad (6) \\
&(\partial_t \tilde{\boldsymbol{u}}, \tilde{\boldsymbol{v}}) + \sum_K \langle \boldsymbol{u}_* \cdot \nabla \tilde{\boldsymbol{u}} - \nu \Delta \tilde{\boldsymbol{u}}, \tilde{\boldsymbol{v}} \rangle_K + \sum_K \langle \nu \boldsymbol{n} \cdot \nabla \tilde{\boldsymbol{u}}, \tilde{\boldsymbol{v}} \rangle_{\partial K} \\
&\quad + \sum_K \langle \partial_t \boldsymbol{u}_h + \boldsymbol{u}_* \cdot \nabla \boldsymbol{u}_h - \nu \Delta \boldsymbol{u}_h + \nabla p_h, \tilde{\boldsymbol{v}} \rangle_K \\
&\quad + \sum_K \langle \nu \boldsymbol{n} \cdot \nabla \boldsymbol{u}_h - p_h \boldsymbol{n}, \tilde{\boldsymbol{v}} \rangle_{\partial K} = \langle \boldsymbol{f}, \tilde{\boldsymbol{v}} \rangle. \qquad (7)
\end{aligned}
$$

These discrete variational equations must hold for all test functions $[\boldsymbol{v}_h, q_h] \in V_h \times Q_h$ and $\tilde{\boldsymbol{v}} \in \tilde{V}$, where $\tilde{V}$ is the space of subscales to be defined. It is observed that some terms have been integrated by parts within each element.

2.3 Simplifying assumptions

Apart from taking the pressure subscale to be zero, no approximations have been made to arrive at (6)-(7). Different approximations will lead precisely to different formulations within the same framework. As mentioned in Section 1, one usually considers $\partial_t \tilde{\boldsymbol{u}} \approx \boldsymbol{0}$ and takes $\boldsymbol{u}_* \approx \boldsymbol{u}_h$ as advection velocity in (6)-(7). However, these are precisely approximations that *we do not necessarily assume*.

Firstly, let us describe the *space of subscales* $\tilde{V}$, that is, the space where $\tilde{\boldsymbol{u}}$ belongs for t fixed. A particular feature of our approach is to take it L^2 *orthogonal to the finite element space*, that is to say, $\tilde{V}$ is taken as a subspace of $V_h^{\perp}$. As it will be mentioned later, this choice has important theoretical consequences.

Next, we will use the approximation $\tilde{\boldsymbol{u}} \approx \boldsymbol{0}$ on ∂K for each element domain K of the finite element partition. That could be understood as approximating the velocity subscale by a space of bubble functions. However, the heuristic Fourier argument proposed in [7] also allows us to explain why the effect of the subscales on the element boundaries can be neglected compared to the effect in the element interiors. Nevertheless, this approximation can be relaxed following the ideas suggested in [11].

Finally, the essential approximation is

$$
\sum_K \langle \boldsymbol{u}_* \cdot \nabla \tilde{\boldsymbol{u}} - \nu \Delta \tilde{\boldsymbol{u}}, \tilde{\boldsymbol{v}} \rangle_K \approx \sum_K \tau_K^{-1} \langle \tilde{\boldsymbol{u}}, \tilde{\boldsymbol{v}} \rangle_K, \qquad (8)
$$

where τ_K is a set of algorithmic parameters computed within each element K as

$$\tau_K^{-1} = \frac{c_1 \nu}{h_K^2} + \frac{c_2 \|\boldsymbol{u}_*\|_{L^\infty(K)}}{h_K}. \tag{9}$$

Here, h_K is a characteristic length of K and c_1 and c_2 are algorithmic constants that depend only on the degree of the finite element approximation being used.

Expression (9) can be motivated also by a heuristic Fourier analysis [7]. In fact, what is important is its asymptotic behavior in terms of h_K, ν and $\|\boldsymbol{u}_*\|_{L^\infty(K)}$. We also would like to stress that the introduction of τ_K comes from the approximation of a *spatial* operator, as it is clearly seen from (8). Therefore, we never include a dependence of τ_K on the temporal discretization.

2.4 Final formulation

The approximations described allow us to formulate a method that can be effectively implemented and that is the formulation we propose. It consists of finding $\boldsymbol{u}_h \in L^2(0,T;V_h)$ and $p_h \in \mathcal{D}'(0,T;Q_h)$ such that

$$\begin{aligned}
&(\partial_t \boldsymbol{u}_h, \boldsymbol{v}_h) + \langle \boldsymbol{u}_* \cdot \nabla \boldsymbol{u}_h, \boldsymbol{v}_h \rangle + \nu(\nabla \boldsymbol{u}_h, \nabla \boldsymbol{v}_h) - (p_h, \nabla \cdot \boldsymbol{v}_h) + (q_h, \nabla \cdot \boldsymbol{u}_h) \\
&\quad - \sum_K \langle \tilde{\boldsymbol{u}}, \boldsymbol{u}_* \cdot \nabla \boldsymbol{v}_h + \nu \Delta \boldsymbol{v}_h + \nabla q_h \rangle_K = \langle \boldsymbol{f}, \boldsymbol{v}_h \rangle, \qquad (10) \\
&(\partial_t \tilde{\boldsymbol{u}}, \tilde{\boldsymbol{v}}) + \sum_K \tau_K^{-1} \langle \tilde{\boldsymbol{u}}, \tilde{\boldsymbol{v}} \rangle_K \\
&\quad + \sum_K \langle \boldsymbol{u}_* \cdot \nabla \boldsymbol{u}_h - \nu \Delta \boldsymbol{u}_h + \nabla p_h, \tilde{\boldsymbol{v}} \rangle_K = \langle \boldsymbol{f}, \tilde{\boldsymbol{v}} \rangle. \qquad (11)
\end{aligned}$$

These equations must hold for all $[\boldsymbol{v}_h, q_h] \in V_h \times Q_h$ and $\tilde{\boldsymbol{v}} \in \tilde{V}$.

A complete numerical analysis of (10)-(11) would include stability and convergence estimates as well as a qualitative analysis of the associated dynamical system. Moreover, in the context of stabilized finite element methods this analysis should be conducted in *norms that do not explode as* $\nu \to 0$ *and allow for any velocity-pressure interpolation*. Whereas the second requirement could be considered not essential by those that favor the use of inf-sup stable velocity-pressure interpolations, the first is a must. From the numerical point of view, estimates that explode with ν are *completely useless* if the formulation is intended to be applied to large Reynolds number flows and, obviously, to model turbulence.

We are still far from the objective described and, in fact, we are not aware of any numerical formulation even close to the target. Certainly, we have some partial (and minor) results. If convection is not an issue and the only concern is the pressure interpolation, we have stability and convergence estimates for the stationary counterpart of (10)-(11) in [9] and for a first order time discretization in [4]. The linearized stationary problem, accounting also

for convection, is analyzed in full detail in [8], whereas the transient Stokes problem is analyzed in [1].

The following two sections describe aspects related to the dissipative structure of problem (10)-(11) and its long term stability.

3 Dissipative structure and backscatter

In this section we describe the dissipative structure of the proposed formulation. First, a local balance of energy will allow us to investigate the flow of energy between the finite element component and the subscales (that is to say, between the resolved and the unresolved scales). We will then present a global balance of energy which shows that it is not necessary to use a LES model apart from the one inherent to the numerical approximation described. Finally, we will discuss the possibility of modeling backscatter and show in a numerical example that it can effectively take place.

In order to highlight the importance of taking $\tilde{V}$ orthogonal to V_h, we will also consider the possibility of using (8) in (6)-(7) without this orthogonality enforcement. The L^2 projection from V to $\tilde{V}$ will be denoted by $\tilde{P}$.

3.1 Local kinetic energy balance equations

Let R be a region formed by a patch of elements, and let $\boldsymbol{t}_R$ be the flux on ∂R, which may include both the flux of stresses (tractions) and convective fluxes. For simplicity, suppose that τ is constant (computed with a characteristic velocity and element length, see Section 4). If $\mathcal{L}_u \boldsymbol{v} := \boldsymbol{u}_* \cdot \nabla \boldsymbol{v} - \nu \Delta \boldsymbol{v}$, taking $\boldsymbol{v}_h = \boldsymbol{u}_h$, $q_h = p_h$ and $\tilde{\boldsymbol{v}} = \tilde{\boldsymbol{u}}$ in (6)-(7), using (8) and neglecting the subscales on the interelement boundaries, we get:

$$\begin{aligned} &\frac{1}{2}\frac{\mathrm{d}}{\mathrm{d}t}\|\boldsymbol{u}_h\|_R^2 + \nu\|\nabla \boldsymbol{u}_h\|_R^2 + (\partial_t \tilde{\boldsymbol{u}}, \tilde{P}(\boldsymbol{u}_h))_R \\ &\quad + \sum_{K \subset R} \langle \tilde{\boldsymbol{u}}, \tilde{P}(\mathcal{L}_u^* \boldsymbol{u}_h - \nabla p_h)\rangle_K = W_R(\boldsymbol{u}_h), \end{aligned} \tag{12}$$

$$\begin{aligned} &\frac{1}{2}\frac{\mathrm{d}}{\mathrm{d}t}\|\tilde{\boldsymbol{u}}\|_R^2 + \tau^{-1}\|\tilde{\boldsymbol{u}}\|_R^2 + (\tilde{P}(\partial_t \boldsymbol{u}_h), \tilde{\boldsymbol{u}})_R \\ &\quad + \sum_{K \subset R} \langle \tilde{\boldsymbol{u}}, \tilde{P}(\mathcal{L}_u \boldsymbol{u}_h + \nabla p_h)\rangle_K = \langle \boldsymbol{f}, \tilde{\boldsymbol{u}}\rangle_R, \end{aligned} \tag{13}$$

where $W_R(\boldsymbol{u}_h) = \langle \boldsymbol{f}, \boldsymbol{u}_h\rangle_R + \langle \boldsymbol{t}_R, \boldsymbol{u}_h\rangle_{\partial R}$ and $\mathcal{L}_u^* \boldsymbol{v} := -\boldsymbol{u}_* \cdot \nabla \boldsymbol{v} - \nu \Delta \boldsymbol{v}$. In (12) we have neglected the term $\langle \boldsymbol{u}_* \cdot \nabla \boldsymbol{u}_h, \boldsymbol{u}_h\rangle$. If $\boldsymbol{u}_*$ is not divergence free (and it is not in the approximated problem), the term $\langle \boldsymbol{u}_* \cdot \nabla \boldsymbol{u}_h, \boldsymbol{v}_h\rangle$ in (6) can be replaced by the skew-symmetric form

$$\begin{aligned} &\frac{1}{2}\langle \boldsymbol{u}_* \cdot \nabla \boldsymbol{u}_h, \boldsymbol{v}_h\rangle - \frac{1}{2}\langle \boldsymbol{u}_* \otimes \boldsymbol{u}_h, \nabla \boldsymbol{v}_h\rangle \\ &\quad = \langle \boldsymbol{u}_* \cdot \nabla \boldsymbol{u}_h, \boldsymbol{v}_h\rangle + \frac{1}{2}\langle \nabla \cdot \boldsymbol{u}_*, \boldsymbol{u}_h \cdot \boldsymbol{v}_h\rangle - \frac{1}{2}\langle \boldsymbol{n} \cdot \boldsymbol{u}_*, \boldsymbol{u}_h \cdot \boldsymbol{v}_h\rangle_\Gamma \end{aligned}$$

without altering the stability and consistency of the formulation. The last term in this expression has been kept to show that only the definition of the flux $\boldsymbol{t}_R$ will change if the integral is performed in a region R interior to Ω.

From (12)-(13) we may draw the first important conclusion. Suppose that $\nu\Delta\boldsymbol{u}_h$ is negligible (because $\boldsymbol{u}_h$ is linear within each element or because ν is very small or because $\tilde{P}(\Delta\boldsymbol{u}_h)\approx\boldsymbol{0}$, as we will see below). Let us define

$$
\begin{aligned}
\mathcal{K}_h &:= \frac{1}{2}\|\boldsymbol{u}_h\|_R^2, \quad \tilde{\mathcal{K}} := \frac{1}{2}\|\tilde{\boldsymbol{u}}\|_R^2 && \text{Kinetic energy of } \boldsymbol{u}_h \text{ and of } \tilde{\boldsymbol{u}}\\
\mathcal{M}_h &:= \nu\|\nabla\boldsymbol{u}_h\|_R^2, \quad \tilde{\mathcal{M}} := \tau^{-1}\|\tilde{\boldsymbol{u}}\|_R^2 && \text{Dissipation of } \boldsymbol{u}_h \text{ and of } \tilde{\boldsymbol{u}}\\
\mathcal{P}_h &:= W_R(\boldsymbol{u}_h), \quad \tilde{\mathcal{P}} := \langle \boldsymbol{f}, \tilde{\boldsymbol{u}}\rangle_R && \text{External power on } \boldsymbol{u}_h \text{ and on } \tilde{\boldsymbol{u}}\\
\mathcal{T} &:= \sum_{K\subset R} \langle \tilde{\boldsymbol{u}}, \tilde{P}(\mathcal{L}_u^*\boldsymbol{u}_h - \nabla p_h)\rangle_K && \text{Energy transfer}
\end{aligned}
$$

Note that the energy transfer term $\mathcal{T}$, when considered in the equation for the finite element component, can be thought as the *numerical dissipation of the formulation.*

From (12)-(13) we see that only if $\tilde{V}$ is a subspace of $V_h^\perp$ the energy balance in region R can be written as

$$
\boxed{
\begin{aligned}
\frac{\mathrm{d}}{\mathrm{d}t}\mathcal{K}_h + \mathcal{M}_h + \mathcal{T} &= \mathcal{P}_h\\
\frac{\mathrm{d}}{\mathrm{d}t}\tilde{\mathcal{K}} + \tilde{\mathcal{M}} - \mathcal{T} &= \tilde{\mathcal{P}}
\end{aligned}
} \tag{14}
$$

Therefore, *there is a scale separation in the kinetic energy balance only if the subscales are orthogonal to the finite element space.*

3.2 Global kinetic energy balance equations

Our thesis that the numerical approximation of the velocity subscales defines a LES model is sustained not only by numerical experiments, but also by some physical reasoning. We present one of these physical arguments next.

For the following discussion we may assume quasi-static subscales (an important implication of considering dynamics subscales is presented in the next subsection) and no body forces applied to the fluid. Neglecting $\nu\Delta\boldsymbol{u}_h$ and calling $\tilde{P} = P_h^\perp$ the projection orthogonal to the finite element space V_h, from (11) it follows that

$$
\tilde{\boldsymbol{u}} = -\tau P_h^\perp(\boldsymbol{u}_*\cdot\nabla\boldsymbol{u}_h + \nabla p_h),
$$

so that the energy balance equation (12) when $R=\Omega$ yields

$$
\frac{1}{2}\frac{\mathrm{d}}{\mathrm{d}t}\|\boldsymbol{u}_h\|^2 + \nu\|\nabla\boldsymbol{u}_h\|^2 + \int_\Omega \varepsilon_{\mathrm{num}} = 0, \tag{15}
$$

where

$$\varepsilon_{\text{num}} := \tau |P_h^{\perp}(\boldsymbol{u}_* \cdot \nabla \boldsymbol{u}_h + \nabla p_h)|^2 \geq 0 \tag{16}$$

is the global numerical dissipation at each point. We may now compare the energy budget (15) with what would be obtained for the continuous problem, using a LES model and approximating numerically a LES model. Let ε_{LES} be the pointwise dissipation associated to a certain LES model (see [22]) and $\bar{\boldsymbol{u}}$ the filtered velocity field resulting from this model. If the LES model is approximated numerically, let $\bar{\boldsymbol{u}}_h$ be the approximation to $\bar{\boldsymbol{u}}$, $\varepsilon_{\text{LES}}^h$ the approximation to the LES dissipation and $\bar{\varepsilon}_{\text{num}}$ the numerical dissipation inherent to the scheme, for example (16) replacing $\boldsymbol{u}_h$ by $\bar{\boldsymbol{u}}_h$ if the formulation we propose is used.

The counterpart of (15) for the continuous problem, a LES model and a numerical approximation of a LES model would respectively be:

$$\frac{1}{2}\frac{\mathrm{d}}{\mathrm{d}t}\|\boldsymbol{u}\|^2 + \int_\Omega \varepsilon_{\text{mol}} = 0, \qquad \varepsilon_{\text{mol}} = \nu|\nabla \boldsymbol{u}|^2, \tag{17}$$

$$\frac{1}{2}\frac{\mathrm{d}}{\mathrm{d}t}\|\bar{\boldsymbol{u}}\|^2 + \nu\|\nabla\bar{\boldsymbol{u}}\|^2 + \int_\Omega \varepsilon_{\text{LES}} = 0, \tag{18}$$

$$\frac{1}{2}\frac{\mathrm{d}}{\mathrm{d}t}\|\bar{\boldsymbol{u}}_h\|^2 + \nu\|\nabla\bar{\boldsymbol{u}}_h\|^2 + \int_\Omega \bar{\varepsilon}_{\text{num}} + \int_\Omega \varepsilon_{\text{LES}}^h = 0. \tag{19}$$

Let us discuss Lilly's argument [20]. Suppose that the flow is turbulent, with fully developed and isotropic turbulence, and that a LES model is used to capture the main flow features. In the inertial range of the Kolmogorov spectrum one may assume that all the kinetic energy of the flow is contained in the large scales, and that the molecular dissipation of these scales is negligible, that is,

$$\frac{\mathrm{d}}{\mathrm{d}t}\|\boldsymbol{u}\|^2 \sim \frac{\mathrm{d}}{\mathrm{d}t}\|\bar{\boldsymbol{u}}\|^2, \qquad \nu\|\nabla\bar{\boldsymbol{u}}\|^2 \sim 0.$$

Comparing the localized versions of (17) and (18) it turns out that these assumptions imply

$$\varepsilon_{\text{LES}}(\bar{\boldsymbol{u}}) \sim \varepsilon_{\text{mol}}(\boldsymbol{u}). \tag{20}$$

This is the basic requirement of a LES model: the dissipation it introduces must be proportional (equal, in the best case) to the molecular dissipation.

The question now is whether the numerical dissipation (16) satisfies this requirement. It is shown in [15] that *if the mesh size h belongs to the inertial range and the classical assumptions of statistical fluid mechanics apply (as described for example in [21]), then*

$$\varepsilon_{\text{num}}(\boldsymbol{u}_h) \sim \varepsilon_{\text{mol}}(\boldsymbol{u}). \tag{21}$$

Furthermore, like in LES models we may consider that $\boldsymbol{u}_h$ carries all (or most of) the kinetic energy of the flow. In this case, the energy balance equations (15) and (18) are formally identical. Moreover, if (20) and (21) both hold, from (19) it follows that *approximating a LES model with a numerical scheme with a dissipation satisfying (21) is clearly redundant.* Of course the numerical approximation is unavoidable. Hence, what is unnecessary is the use of a LES model.

3.3 Backscatter

In this subsection we use again a heuristic reasoning to analyze the possibility to model backscatter by our numerical formulation.

Using the notation introduced heretofore, backscatter can be defined by condition $\mathcal{T} < 0$, where $\mathcal{T}$ is the energy transfer term appearing in (14). This means that energy is supplied from the unresolved (small) scales to the resolved (finite element) scales. Physically, it is known that this can happen only at isolated spatial points and time instants. Numerically, the model should be such that $\mathcal{T}$ can be negative only if region R is small enough (possibly a single element) and at a few time steps of the time discretization.

As before, we will consider the subscales orthogonal to the finite element space and that $\boldsymbol{f} \in V_h$. From (11) we have that

$$\tilde{\boldsymbol{u}} = -\tau[\partial_t \tilde{\boldsymbol{u}} + \tilde{P}(\mathcal{L}_u \boldsymbol{u}_h + \nabla p_h)],$$

which upon substitution in the expression of $\mathcal{T}$ yields

$$\mathcal{T} = \underbrace{\sum_{K \subset R} \tau \langle \tilde{P}(\mathcal{L}_u \boldsymbol{u}_h + \nabla p_h), \tilde{P}(-\mathcal{L}_u^* \boldsymbol{u}_h + \nabla p_h) \rangle_K}_{(\int_R \varepsilon_{\text{num}})} + \underbrace{\sum_{K \subset R} \tau \langle \partial_t \tilde{\boldsymbol{u}}, \tilde{P}(-\mathcal{L}_u^* \boldsymbol{u}_h + \nabla p_h) \rangle_K}_{(\int_R \beta_{\text{num}})}.$$

If viscous terms are negligible (or $\Delta \boldsymbol{v}_h$ is approximated by the discrete Laplacian $\Delta_h \boldsymbol{v}_h$) and $\boldsymbol{r} = -P_h^{\perp}(\boldsymbol{u}_* \cdot \nabla \boldsymbol{u}_h + \nabla p_h)$ we have

$$\mathcal{T} = \int_R \varepsilon_{\text{num}} + \int_R \beta_{\text{num}} = \sum_K \tau \left(\langle \boldsymbol{r}, \boldsymbol{r} \rangle_K - \langle \partial_t \tilde{\boldsymbol{u}}, \boldsymbol{r} \rangle_K \right). \tag{22}$$

From this expression it immediately follows that *when orthogonal subscales are used, backscatter is possible only if the subscales are dynamic*, since otherwise the second term in (22) vanishes and the first one is obviously non-negative. If the time derivative of the subscales is included in (22), *nothing can be said about the sign of* $\mathcal{T}$, and therefore the possibility to model backscatter is open.

However, the numerical model will be physically admissible if $\mathcal{T}$ is, in a certain average sense, non-negative. This is what we will justify now heuristically.

Assume $\boldsymbol{r}$ is periodic in t, of period T_0, and so is $\tilde{\boldsymbol{u}}$. If

$$\boldsymbol{r}(\boldsymbol{x},t) = \sum_{n=0}^{\infty}(A_n(\boldsymbol{x})\cos(\omega_n t) + B_n(\boldsymbol{x})\sin(\omega_n t)), \quad \omega_n = \frac{2\pi n}{T_0},$$
$$\tilde{\boldsymbol{u}}(\boldsymbol{x},t) = \sum_{n=0}^{\infty}(\tilde{A}_n(\boldsymbol{x})\cos(\omega_n t) + \tilde{B}_n(\boldsymbol{x})\sin(\omega_n t)),$$

imposing

$$\partial_t\tilde{\boldsymbol{u}} + \tau^{-1}\tilde{\boldsymbol{u}} = \boldsymbol{r}(t),$$

it is found that

$$\tilde{A}_n(\boldsymbol{x}) = \frac{A_n\tau^{-1} - B_n\omega_n}{\tau^{-2}+\omega_n^2}, \quad \tilde{B}_n(\boldsymbol{x}) = \frac{A_n\omega_n + B_n\tau^{-1}}{\tau^{-2}+\omega_n^2}.$$

Averaging over a period and assuming τ constant in region R we get

$$\begin{aligned}\frac{1}{T_0}\int_0^{T_0}\mathcal{T}\,\mathrm{d}t &= \frac{1}{T_0}\int_0^{T_0}\int_R(\varepsilon_{\mathrm{num}}+\beta_{\mathrm{num}})\mathrm{d}t\\ &= \frac{\tau}{T}\int_0^T\sum_K\left(\langle\boldsymbol{r},\boldsymbol{r}\rangle_K - \langle\partial_t\tilde{\boldsymbol{u}},\boldsymbol{r}\rangle_K\right)\mathrm{d}t\\ &= \tau\int_R\sum_{n=0}^{\infty}\frac{1}{1+(\omega_n\tau)^{-2}}(A_n^2+B_n^2).\end{aligned}$$

If $\beta_{\mathrm{num}} = 0$ (quasi-static subscales) the result we would have obtained is the same without the term $(\omega_n\tau)^{-2}$, from where we may conclude that $\int_R\beta_{\mathrm{num}}$ can be negative. However, even though the average energy transfer is smaller with dynamic subscales, *it is, on average, positive*. Thus, this physical restriction holds in the case considered, regardless of the period T_0.

3.4 Flow over a surface mounted obstacle

We close this section with a numerical experiment showing that *backscatter can certainly be found in numerical experiments*. This example is taken from [23], to which the reader is referred for details of the calculation.

The problem consists in modeling the flow over a surface mounted obstacle, consisting in a cylinder of square cross section. Just to have a feeling of the flow, the time-averaged iso-velocity contours and the instantaneous velocity contours in the mid section of the channel where the flow takes place are plotted in Fig. 1. The numerical dissipation $\mathcal{T}$ averaged over time in the same section is shown in Fig. 2. It is observed that it is more localized using dynamic subscales that quasi-static subscales.

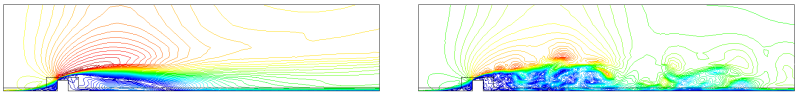

Fig. 1. Averaged velocity field (left) and instantaneous velocity field (right)

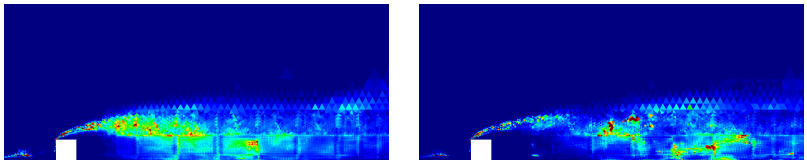

Fig. 2. Averaged numerical dissipation obtained with quasi-static subscales (left) and with dynamic subscales (right)

The interesting fact of this numerical simulation is that backscatter is found, obviously using dynamic subscales (no backscatter can be found with quasi-static subscales). If we compute the numerical dissipation $\mathcal{T}$ for each element and at each time step of the time discretization, it turns out that it is negative at some elements and some time steps. In Fig. 3 the elements where this happens at a certain time step are marked in red.

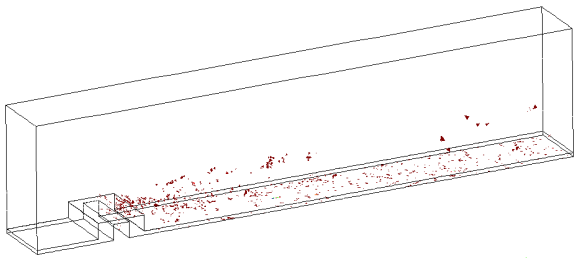

Fig. 3. Elements with instantaneous negative numerical dissipation using dynamic subscales

4 Long term stability

In this section we present the results of a complete stability analysis we have performed for formulation (10)-(11), which can be found in [2]. We will state the stability result for both $T < \infty$ and $T = \infty$, which is our main interest.

Our analysis is based in fact on a simplified version of (10)-(11). First, we assume orthogonal subscales (we envisage a lot of difficulties in the analysis if this is not assumed). This allows us to delete the viscous operator in the terms involving the subscales in (10)-(11). In the case of orthogonal subscales, this does not deteriorate the consistency and stability of the formulation [8]. We may think for example that $\Delta \boldsymbol{v}_h|_K$ is approximated by the discrete Laplacian $\Delta_h \boldsymbol{v}_h|_K$, and therefore $P_h^{\perp}(\Delta \boldsymbol{v}_h|_K) \approx P_h^{\perp}(\Delta_h \boldsymbol{v}_h|_K) = \boldsymbol{0}$.

The two real additional assumptions that we make are the following:

- $\boldsymbol{u}_* \approx \boldsymbol{u}_h$ as advection velocity.
- $\forall K\ \tau_K^{-1} = \tau^{-1} = \frac{c_1 \nu}{h^2} + \frac{c_2 U}{h}$, where $U = \frac{\|\boldsymbol{u}_h\|_{L^p(\Omega)}}{|\Omega|^{1/p}}$, with $2 < p < \infty$.

The first assumption simplifies greatly the nonlinearity of the problem. The second basically states that a single τ is used for the whole computational domain. This will weaken the strength of the results to be presented, but nevertheless they are important enough, as we will see.

With the assumptions described, the method reduces to

$$(\partial_t \boldsymbol{u}_h, \boldsymbol{v}_h) + \langle \boldsymbol{u}_h \cdot \nabla \boldsymbol{u}_h, \boldsymbol{v}_h \rangle + \nu(\nabla \boldsymbol{u}_h, \nabla \boldsymbol{v}_h) - (p_h, \nabla \cdot \boldsymbol{v}_h) + (q_h, \nabla \cdot \boldsymbol{u}_h) - \langle \tilde{\boldsymbol{u}}, \boldsymbol{u}_h \cdot \nabla \boldsymbol{v}_h + \nabla q_h \rangle = \langle \boldsymbol{f}, \boldsymbol{v}_h \rangle, \tag{23}$$

$$(\partial_t \tilde{\boldsymbol{u}}, \tilde{\boldsymbol{v}}) + \tau^{-1} \langle \tilde{\boldsymbol{u}}, \tilde{\boldsymbol{v}} \rangle + \langle \boldsymbol{u}_h \cdot \nabla \boldsymbol{u}_h + \nabla p_h, \tilde{\boldsymbol{v}} \rangle = \langle \boldsymbol{f}, \tilde{\boldsymbol{v}} \rangle, \tag{24}$$

which must hold for all test functions $[\boldsymbol{v}_h, q_h]$, $\tilde{\boldsymbol{v}}$, and in the time interval $[0, T]$.

Estimates for $T < \infty$.

Formally (see [2] for technical details) we may take $\boldsymbol{v}_h = \boldsymbol{u}_h$, $q_h = p_h$, $\tilde{\boldsymbol{v}} = \tilde{\boldsymbol{u}}$ in (23)-(24). Integrating then on $[0, t']$, $t' \leq T$, one gets:

$$\|\boldsymbol{u}_h(t')\|^2 + \|\tilde{\boldsymbol{u}}(t')\|^2 + \int_0^{t'} \nu \|\nabla \boldsymbol{u}_h\|^2 \mathrm{d}t + \int_0^{t'} \tau^{-1} \|\tilde{\boldsymbol{u}}\|^2 \mathrm{d}t \leq \int_0^{t'} \frac{1}{\nu} \|\boldsymbol{f}\|_{-1}^2 \mathrm{d}t + \|\boldsymbol{u}^0\|^2,$$

from where

$$\boxed{\begin{array}{l} \|\boldsymbol{u}_h\| \in L^\infty(0,T), \quad \nu^{1/2} \|\nabla \boldsymbol{u}_h\| \in L^2(0,T), \\ \|\tilde{\boldsymbol{u}}\| \in L^\infty(0,T), \quad \tau^{-1/2} \|\tilde{\boldsymbol{u}}\| \in L^2(0,T). \end{array}} \tag{25}$$

The interest of these estimates is that we obtain *the same bounds for the finite element component as for the Galerkin method plus additional stability on the subscales*. This is also true for the estimates presented next. In [2] it is shown how to translate the stability obtained for the subscales to additional stability for the finite element component.

Estimates in $L^\infty(0,\infty;L^2(\Omega)^d)$.

In this case our analysis strategy is similar to that used for continuous problems (see for example [24]). Taking $\boldsymbol{v}_h = \boldsymbol{u}_h$, $q_h = p_h$, $\tilde{\boldsymbol{v}} = \tilde{\boldsymbol{u}}$ in (23)-(24) and using the classical Gronwall lemma it is found that

$$\boxed{\|\boldsymbol{u}_h\| \in L^\infty(0,\infty), \quad \|\tilde{\boldsymbol{u}}\| \in L^\infty(0,\infty).} \tag{26}$$

Similar remarks to those made for (25) apply to (26). In this case we can also prove that

$$\lim_{t\to\infty} \sup \left(\|\boldsymbol{u}_h\| + \|\tilde{\boldsymbol{u}}\|\right) \leq C \frac{|\Omega|^{2/d}}{\nu} \|\boldsymbol{f}\|_{L^\infty(0,\infty;L^2(\Omega)^d)},$$

from which we conclude that:

- There is a $L^2(\Omega)\oplus L^2(\Omega)$-absorbing set in $V_h \oplus \tilde{V}$ (not only in V_h).
- The diameter of this absorbing set is bounded by the Reynolds number, Re (or, equivalently, by $1/\nu$).

Estimates in $L^\infty(0,\infty;H^1(\Omega)^2)$ *(case* $d=2$*).*

Finally, we can prove estimates in the strong norm of $L^\infty(0,\infty;H^1(\Omega)^2)$. As for the continuous problem, this is only possible in the two-dimensional case.

Let $\tau_0^{-1} = \frac{\nu}{h^2} + \frac{U_0}{h}$, where $U_0 \leq U$ is a characteristic velocity. Using the uniform Gronwall lemma it is found that

$$\boxed{\nu^{1/2}\|\nabla \boldsymbol{u}_h\| \in L^\infty(0,\infty), \quad \tau_0^{-1/2}\|\tilde{\boldsymbol{u}}\| \in L^\infty(0,\infty).} \tag{27}$$

Once again, we obtain stability not only for the finite element component, but also for the subscales.

Define now the quantities

$$\begin{aligned}
a_1 &:= \tilde{t}\left(\|\boldsymbol{f}\|^2_{L^\infty(0,\infty;L^2(\Omega)^d)} + U_0^4\right),\\
a_2 &:= (\nu^{-1}|\Omega| + \tilde{t})\nu^{-1}|\Omega|\|\boldsymbol{f}\|^2_{L^\infty(0,\infty;L^2(\Omega)^d)},\\
a_3 &:= \nu^{-2}(\nu^{-4}|\Omega|^2\|\boldsymbol{f}\|^2_{L^\infty(0,\infty;L^2(\Omega)^d)} + 1)a_2.
\end{aligned}$$

Then, it can be shown that

$$\lim_{t\to\infty} \sup \left(\nu\|\nabla \boldsymbol{u}_h\|^2 + \tau_0^{-1}\|\tilde{\boldsymbol{u}}\|^2\right) \leq C\left(a_1 + \frac{a_2}{\tilde{t}}\right)\exp(a_3),$$

from where conclude that

- There is a $H^1(\Omega)\oplus \tilde{H}(\Omega)$-absorbing set in $V_h \oplus \tilde{V}$, where $\tilde{H}(\Omega) = \tau_0^{-1/2}L^2(\Omega)$.

- The diameter of this absorbing set is bounded by $\exp(\mathrm{Re}^4)$. This is useless from the numerical point of view, but
- Since $H^1(\Omega)$ is compact in $L^2(\Omega)$, the $L^2(\Omega)$-absorbing set in V_h is in fact an attractor.

The general conclusion of all these results is that the long term dynamics engendered by the numerical formulation (23)-(24) are what one could expect. To obtain all these results, particularly estimates in $L^\infty(0,T)$ (including the case $T=\infty$) it is crucial to have the time derivative of the subscales, that is to say, the subscales need to be dynamic.

5 Long term simulations

In this section we present without details the results of two numerical simulations with the objective of comparing the performance of (10)-(11) for fully developed turbulent flows with LES models. Since our claim is that these models are not necessary, we will compare the results obtained with and without one of them, in particular Smagorinsky's model. In this case, a turbulent viscosity $\nu_{\mathrm{LES}} = 0.01h^2(\nabla^S \boldsymbol{u}_h : \nabla^S \boldsymbol{u}_h)^{1/2}$ is added to the molecular viscosity ν.

5.1 Flow over a plate

The first example is the flow over a circular plate supported on a column and inclined. This example has been taken from [15], which may be consulted for details. Again, Fig. 4 shows some results of the numerical simulation to provide a qualitative feeling of the flow.

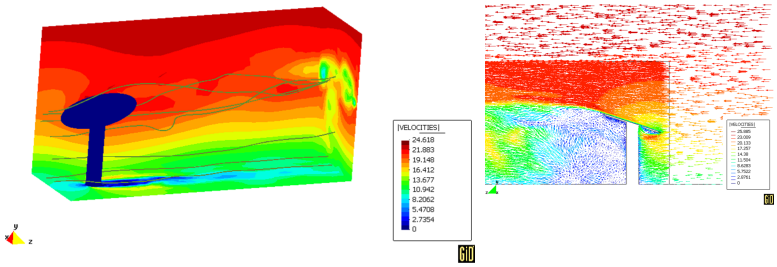

Fig. 4. Left: pressure contours and some particle trajectories. Right: velocity field in the mid section

What we wish to compare in this example is the Kolmogorov spectrum obtained with and without Smagorinky's model. The pressure spectra at the center of the plate obtained in both cases are shown in Fig. 5. It is observed that in both cases the $-7/3$ slope is well approximated. In fact, these spectra agree well with experimental results [15]. The interesting fact is that, even

though both spectra are similar, the dynamical behavior obtained *without* Smagorinky's model is richer that with it, as it could be expected. This is a general trend that we have observed and demonstrated in Fig. 5 (right), where a window of the temporal evolution of the pressure at the center of plate is depicted.

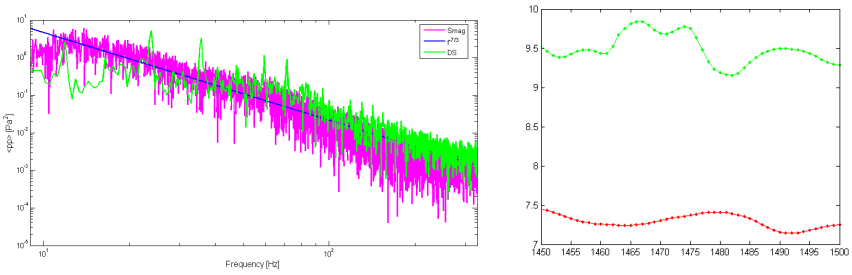

Fig. 5. Comparison of dynamic subscales (green in both pictures) and quasi-static subscales with Smagorinsky's model. Left: numerical pressure spectra (theoretical slope $= -7/3$), right: detail of the pressure evolution (at the center of the plate)

5.2 Flow around a telescope

The second example we present is intended to demonstrate that (10)-(11) is indeed applicable to real flow problems. It consists in the aerodynamic analysis around a building enclosing a large telescope. Modeling turbulence is crucial to determine the optical quality of the site where the telescope is placed.

The geometry of the building and the finite element mesh used to discretize it are shown in Fig. 6. To understand the behavior of the flow, Fig. 7 shows the velocity vectors at a certain time of the calculation and the pressure contours, as well as the trajectories of some particles.

The scientifically relevant issue is whether the model is able to capture the inertial range of the Kolmogorov spectrum. The pressure spectra at a point inside the building for different flow conditions are shown in Fig. 8. It is observed that these spectra display the correct $-7/3$ slope.

In order to compare the results obtained with Smagorinsky's model (SMA) with quasi-static subscales, quasi-static subscales without Smagorinsky's model (QSS) and dynamic subscales without Smagorinsky's model (DS), we have listed in Table 1 some parameters of the turbulence along a vertical line in the middle of the telescope enclosure. In particular, values for the mean velocity U and turbulence intensity I, defined by

$$U(\boldsymbol{x}) := \frac{1}{T}\int_0^T |\boldsymbol{u}_h(\boldsymbol{x},t)|\,\mathrm{d}t, \quad I^2(\boldsymbol{x}) := \frac{1}{U^2(\boldsymbol{x})T}\int_0^T (|\boldsymbol{u}_h(\boldsymbol{x},t)| - U(\boldsymbol{x}))^2\,\mathrm{d}t \tag{28}$$

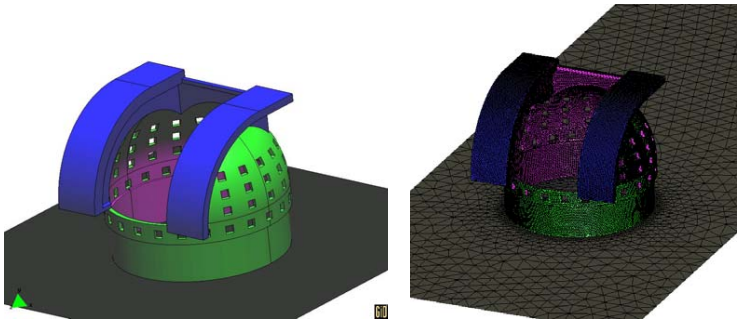

Fig. 6. Geometry of telescope enclosure (left) and the surface mesh for the numerical approximation (right).

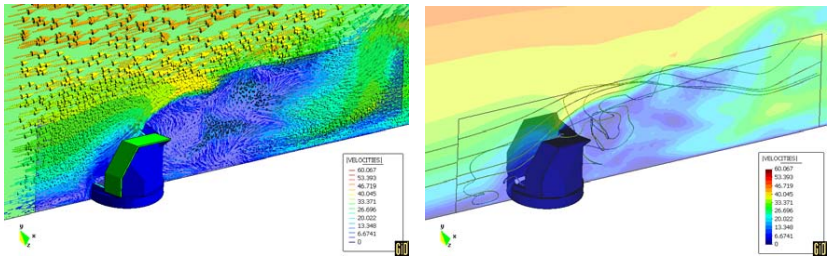

Fig. 7. Contours of velocity norm, together with velocity vectors (left) and pressure contours, together with some particle trajectories (right) for the flow over a telescope enclosure

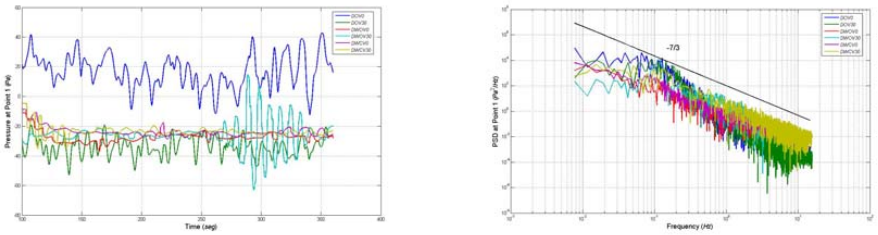

Fig. 8. Pressure history and pressure spectrum at a point inside the enclosure for different flow conditions

are listed in Table 1 against the height (H) of the point to the ground. In (28), T is a time window, large enough to consider the results (almost) stationary.

H	U SMA	U QSS	U DS	I SMA	I QSS	I DS
6.93	1.06	1.08	1.21	0.18	0.21	0.20
13.08	1.00	1.02	1.01	0.23	0.25	0.25
19.70	1.61	1.64	1.65	0.46	0.55	0.54
26.65	5.19	5.25	5.33	0.08	0.11	0.11
32.86	5.27	5.26	5.25	0.03	0.06	0.06
39.44	3.21	3.22	3.44	0.09	0.11	0.12
46.13	1.89	1.99	2.05	0.17	0.35	0.33
52.51	1.58	1.67	1.98	0.25	0.44	0.44
59.41	1.37	1.44	1.40	0.22	0.43	0.42
66.12	1.08	1.07	1.04	0.35	0.67	0.65
72.13	0.87	1.02	1.01	0.30	0.41	0.42

Table 1. Mean velocity and turbulence intensity along a vertical line inside the telescope enclosure

As expected, results are much more dissipative using Smagorinsky's model than without it. However, there is no clear trend in whether QSS is more or less dissipative that DS. In fact, results in this case are very similar.

6 Conclusions

In this work we have summarized the formulation we have been developing to approximate the incompressible Navier-Stokes equations. We have also explained some of its features related to the simulation of fully developed turbulent flows and long term stability.

The key ingredients of our formulation are

- time dependent subgrid scales,
- contribution from the subscales in the advection velocity,
- subgrid scales orthogonal to the finite element space,

together with a certain definition of the stabilization parameter. These ingredients are essential to obtain analytically:

- the correct dissipative structure (balance of energy between resolvable and subgrid scales),
- a numerical dissipation proportional to the molecular one (which poses the question on the need to use LES models),
- the possibility to model backscatter,
- correct weak and strong stability estimates in the long term.

Numerical experiments show that:

- the numerical solution is stable in the long term,
- backscatter can certainly be found,
- the $-7/3$ pressure spectrum slope in the inertial range can be observed *without* using any LES model.

Acknowledgments

Several people have participated in the research presented here. In particular, Oriol Guasch and Juan V. Gutiérrez-Santacreu have collaborated closely in the results presented in [15, 12] and [2], respectively, and summarized here. The participation of Florian Henke, Daniel Pérez-Sánchez and Christian Muñoz in the elaboration of the numerical results is also acknowledged. The numerical results presented in Section 5 have been conducted in the context of project *ELT-DS Technology development programme towards a European Extremely Large Telescope*, within the FP6-2003 of the European Comission.

References

1. S. Badia and R. Codina. On a multiscale approach to the transient Stokes problem. Transient subscales and anisotropic space-time discretization. *Applied Mathematics and Computation*, 207:415–433, 2009.
2. S. Badia, R. Codina, and J.V. Gutiérrez-Santacreu. Long term stability estimates and existence of global attractors in a finite element approximation of the Navier-Stokes equations with numerical sub-grid scale modeling. Submitted.
3. Y. Bazilevs, V.M. Calo, J.A. Cottrell, T.J.R. Hughes, A. Reali, and G. Scovazzi. Variational multiscale residual-based turbulence modeling for large eddy simulation of incompressible flows. *Computer Methods in Applied Mechanics and Engineering*, 197:173–201, 2007.
4. J. Blasco and R. Codina. Space and time error estimates for a first order, pressure stabilized finite element method for the incompressible Navier-Stokes equations. *Applied Numerical Mathematics*, 38:475–497, 2001.
5. R. Codina. Comparison of some finite element methods for solving the diffusion-convection-reaction equation. *Computer Methods in Applied Mechanics and Engineering*, 156:185–210, 1998.
6. R. Codina. A stabilized finite element method for generalized stationary incompressible flows. *Computer Methods in Applied Mechanics and Engineering*, 190:2681–2706, 2001.
7. R. Codina. Stabilized finite element approximation of transient incompressible flows using orthogonal subscales. *Computer Methods in Applied Mechanics and Engineering*, 191:4295–4321, 2002.
8. R. Codina. Analysis of a stabilized finite element approximation of the Oseen equations using orthogonal subscales. *Applied Numerical Mathematics*, 58:264–283, 2008.
9. R. Codina and J. Blasco. Analysis of a pressure-stabilized finite element approximation of the stationary Navier-Stokes equations. *Numerische Mathematik*, 87:59–81, 2000.

10. R. Codina and J. Principe. Dynamic subscales in the finite element approximation of thermally coupled incompressible flows. *International Journal for Numerical Methods in Fluids*, 54:707–730, 2007.
11. R. Codina, J. Principe, and J. Baiges. Subscales on the element boundaries in the variational two-scale finite element method. *Computer Methods in Applied Mechanics and Engineering*, 198:838–852, 2009.
12. R. Codina, J. Principe, O. Guasch, and S. Badia. Time dependent subscales in the stabilized finite element approximation of incompressible flow problems. *Computer Methods in Applied Mechanics and Engineering*, 196:2413–2430, 2007.
13. P.A.B. de Sampaio, P.H. Hallak, A.L.G.A. Coutinho, and M.S. Pfeil. A stabilized finite element procedure for turbulent fluid-structure interaction using adaptive time-space refinement. *International Journal for Numerical Methods in Fluids*, 44:673–693, 2004.
14. J. Donéa and A. Huerta. *Finite Element Methods for Flow Problems*. John Wiley & Sons, 2003.
15. O. Guasch and R. Codina. A heuristic argument for the sole use of numerical stabilization with no physical LES modelling in the simulation of incompressible turbulent flows. *UPCommons*, `http://hdl.handle.net/2117/3021`, Submitted.
16. J. Hoffman and C. Johnson. A new approach to computational turbulence modeling. *Computer Methods in Applied Mechanics and Engineering*, 195:2865–2880, 2006.
17. T.J.R. Hughes. Multiscale phenomena: Green's function, the Dirichlet-to-Neumann formulation, subgrid scale models, bubbles and the origins of stabilized formulations. *Computer Methods in Applied Mechanics and Engineering*, 127:387–401, 1995.
18. T.J.R. Hughes, G.R. Feijóo, L. Mazzei, and J.B. Quincy. The variational multiscale method–a paradigm for computational mechanics. *Computer Methods in Applied Mechanics and Engineering*, 166:3–24, 1998.
19. T.J.R. Hughes, L. Mazzei, and K.E. Jansen. Large eddy simulation and the variational multiscale method. *Computing and Visualization in Science*, 3:47–59, 2000.
20. D.K. Lilly. The representation of small-scale turbulence theory in numerical simulation experiments. In H.H. Goldstine, editor, *Proc. IBM Scientific Computing Symp. on Environmental Sciences*, 1967.
21. A.S. Monin and A.M. Yaglom. *Statistical Fluid Mechanics: Mechanics of Turbulence. Volume I*. Cambridge, MA: MIT Press., 1971.
22. S.B. Pope. *Turbulent Flows*. Cambridge University Press, 2000.
23. J. Principe, R. Codina, and F. Henke. The dissipative structure of variational multiscale methods for incompressible flows. *Computer Methods in Applied Mechanics and Engineering*, To appear.
24. R. Temam. *Infinite-dimensional dynamical systems in mechanics and physics*. Springer, 1988.